ACCURACY LIMITS IN NONSTEADY FLIGHT TESTING

Dr. H.L. Jonkers and Ir. J.A. Mulder

Department of Aerospace Engineering
Delft University of Technology
The Netherlands

Abstract

When estimating aircraft performance, stability and control characteristics from steady or nonsteady maneuvering test flight data the accuracy of the results is limited due to measurement errors, atmospheric disturbances and mathematical modelling errors. This paper studies the effects of various error sources on the maximally achievable accuracies of the aircraft characteristics derived from nonsteady maneuvering flight test data.
It is shown which error sources are most relevant for accuracy limitations in present day flight testing, taking account of aerodynamic and inertial aircraft properties.
Conclusions drawn from theoretical analyses are compared with results obtained by processing digitally simulated and actual flight test data.
The material presented is an extension of earlier material published by Gerlach, Hosman, Mulder and Jonkers.

0. Introduction

Experimental evaluation of aircraft flight dynamics is based in general on separately measuring motions of- and about the aircraft's centre of gravity (c.g.).

Traditional performance testing relies on measurement of aircraft c.g. motions in steady state flight conditions, i.e. when the aircraft experiences neither translational nor rotational accelerations. Each set of steady flight conditions selected for performance measurement obviously corresponds with a single performance data point.
As flight performance depends on many variables characterizing aircraft state and configuration a large number of steady flight conditions has to be selected for adequate performance evaluation throughout the entire flight envelope of the test aircraft.

Static and dynamic stability and control characteristics are related in principle to the balance of aerodynamic and inertial moments or to the motions about the aircraft's c.g. These characteristics are either derived from measurements in steady flight conditions or deduced from measured unsteady deviations from steady rectilinear flight, resulting from control surface deflections. Since the stability and control characteristics, such as for example the stability derivatives, vary with the nominal flight condition, a considerable number of nominal conditions should be selected out of the flight envelope of the test aircraft, for determination of the characteristics of interest.

Trimming the aircraft for a preselected steady condition may require several minutes. Each condition has to be maintained during approximately 30 to 60 seconds for performance measurement. Measurement time intervals of the same order of magnitude are required for response measurements. In addition it should be remarked that traditional aircraft performance testing is usually not combined with aircraft stability and control testing. The traditional flight test techniques may thus be concluded to be time consuming and cumbersome.

The accuracy of performance data points may be reduced as a result of difficult and consequently imperfect trimming of the aircraft, atmospheric perturbations and measurement errors. Modern high performance jet transports will offer yet another problem for traditional performance testing, as the rate of climb achievable under various steady flight conditions will result in continually varying atmospheric conditions during a single steady flight. The resulting variations in aerodynamic forces and moments will obviously prohibit establishment of exactly steady flight conditions as required.

Efforts to overcome the flight test problems mentioned, by derivation of aircraft performance in steady flight, from measurements in quasi-steady and nonsteady flight have been reported earlier by Hussenot (1950) [1], Vleghert (1957) [2], Gerlach (1964) [3], Klopfenstein (1965) [4] and Tourraille and Langlade (1971) [5].

The flight test method developed at the Department of Aerospace Engineering of the Delft University of Technology by O.H. Gerlach and his coworkers centers around combined derivation of aircraft performance as well as stability and control characteristics, from a single nominally* symmetric nonsteady maneuvering test flight and highly accurate measurement of inertial and barometric quantities. Objectives of the method developed are:

1. determination of the aircraft's polar drag curve and lift curve,
2. determination of the curves representing rate of climb and elevator angle as a function of airspeed in steady rectilinear flight (amongst others for computation of maximum rate of climb and maximum airspeed),
3. determination of elevator angle per g in steady curvy linear flight,
4. computation of aircraft stability and control derivatives and eigenvalues,

in principle from a combination of quasi-steady and nonsteady flight intervals in a single test flight.

Application of this method for evaluation of aircraft performance as well as stability and control characteristics yields in principle a drastic reduction in the flight test time required and considerably eases the test pilot's job. Combination of performance measurement with stability and control testing in a single nonsteady maneuvering test flight seems most appropriate for modern, large jet transports, because of the increasing complications in traditional flight testing, as resulting from the

* The aircraft's flight path is called nominally symmetric to indicate small asymmetric deviations from the intended strictly symmetric flight.

narrowing gaps between the frequencies characterizing the aircraft's behaviour in steady flight, the phugoid mode, the spiral mode, the short period mode, the Dutch roll mode, low frequency dynamic aeroelastic modes and flutter, see [6].
The nonsteady flight test method developed will be shown to provide accurate flight performance-, stability- and control data, when flight testing low speed, propeller driven, light weight aircraft as well as jet aircraft.

The analysis of nonsteady maneuvering flight test data will be discussed in this paper. The paper is organized as follows.
The flight test data analysis procedure developed will be briefly outlined and motivated in Section 1.
Section 2 will be devoted to the flight path estimation problem and the extraction of aerodynamic model parameters from test flight data.
The principles underlying the derivation of aircraft performance as well as stability and control characteristics from nonsteady maneuvering flight test measurements, flight path reconstruction and aerodynamic model identification results will be discussed briefly in Section 3.
Experimental results obtained by flight testing a low subsonic, propeller driven aircraft are presented and discussed briefly in Section 4.
Experimental results obtained by flight testing a high subsonic jet aircraft are presented and discussed in Section 5.

1. Flight test data analysis procedure

1.0 Procedure outline

To provide an outline of the procedure used for the analysis of nonsteady maneuvering flight test data, [6-9], the following procedure steps are distinguished.

1. The first step includes transformation of transducer output voltages, accurately measured, periodically sampled, digitized and recorded in flight, into the corresponding physical magnitudes, using the results of laboratory calibrations of the flight test instrumentation system.
2. The second procedure step results in accurate reconstruction of the aircraft's motions in nominally symmetric nonsteady maneuvering flight from the flight test measurements recorded including estimation of the time histories of the angle of attack $\alpha(t)$ and the angle of pitch $\theta(t)$ not directly measured in flight.
3. The third procedure step is directed towards the identification of the aircraft's aerodynamic model, [6,7], including specification of the relations between the aircraft's state and control variables and the resulting aerodynamic forces and moments as well as estimation of the constants and aerodynamic derivatives governing these relations.
4. The final step includes the derivation of aircraft performance in steady flight as well as stability and control characteristics either from the aerodynamic model obtained or from the reconstructed state variable time histories of the nonsteady maneuvering test aircraft, [3,6,7,10,11].

1.1 Discussion

Accurate flight path reconstruction from highly accurate but still imperfect flight test measurements, prior to aerodynamic model identification is required for accurate estimation of the angle of pitch $\theta(t)$ and the angle of attack $\alpha(t)$ and improves the accuracy of the model parameters extracted from these data. The angle of attack is estimated from inertial and barometric measurements rather than directly measured with a boom mounted vane to avoid the problem of vane calibration and all inherent static and dynamic measurement errors.

Additional advantages of aerodynamic model identification posterior to accurate flight path reconstruction and estimation of bias error corrections as described in [3,6,7], are robustness, flexibility and computational efficiency of the aerodynamic model identification process.*

The question may arise as to what extent the theoretically seemingly attractive, combined flight path reconstruction and aerodynamic model identification from onboard measurements may yield more accurate results than can be obtained when separating flight path reconstruction from aerodynamic model identification. Separation of flight path reconstruction from aerodynamic model identification can be shown to yield near optimal results if the errors in the measurements of the specific aerodynamic forces A_X and A_Z and the angular acceleration $\dot{q}$ can be assumed negligibly small as compared to the modelling errors in the expressions used for aerodynamic model identification [12]. Very accurate measurement of the specific forces A_X and A_Z with body-fixed accelerometers and the rate of pitch q, with a highly accurate rate gyroscope, followed by careful differentiation of the measured rate of pitch for computation of $\dot{q}$ therefore allows in principle for separation of flight path reconstruction from aerodynamic model identification based on separate modelling of aircraft kinematics and aerodynamics.

In this study regression analysis will be used for the estimation of aerodynamic model parameters from onboard measurements and the subsequent flight path reconstruction results.

The aerodynamic model identified can be used for calculation of aircraft performance, static and dynamic stability and control characteristics throughout the entire flight envelope traversed during flight testing as well as for corrections of quasi-steady flight conditions to steady flight conditions required for estimation of the characteristics of interest from the aircraft's behaviour in quasi-steady flight.

2. Flight path reconstruction and aerodynamic model identification

2.0 Flight path reconstruction

Introduction. Application of the extended Kalman filter and extended Kalman fixed interval smoothing procedure, [10,13,14], to flight path reconstruction from onboard measurements in nominally symmetric

* Robustness of the entire estimation procedure implies insensitivity of flight path reconstruction results to incomplete knowledge of the aerodynamic model.
Flexibility of the model identification algorithms refers to easy model structure variation as required for model design purposes.

nonsteady maneuvering flight, as well as the aerodynamic model identification problems, will be discussed briefly in this section. First of all the dynamic system model used for Kalman estimation procedure design will be discussed.

The system model. The aircraft will be considered as a rigid body flying through an airmass at rest over a flat non-rotating earth.*

All accelerations, velocities, rotation rates and angles relevant with respect to the aircraft's maneuver under consideration are specified in Fig. 2.1, [15].

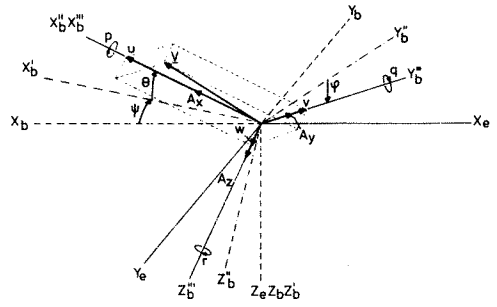

FIG.21: AIRCRAFT ACCELERATIONS, VELOCITIES, ROTATIONS AND ANGLES

The aircraft's motions are assumed nominally symmetric. The magnitudes of the lateral aerodynamic force Y, the lateral component v of the aircraft's airspeed $\underline{V}$ along the Y_b-axis of its body frame F_b, the angle of yaw ψ, the rate of yaw r, the angle of roll φ and the rate of roll p are henceforth assumed negligibly small as compared to the magnitudes of corresponding quantities characterizing symmetric flight.

The aircraft's motions relative to F_b are then described by the following equations:

$$-W \sin \theta + X = m(\dot{u} + qw) \tag{2.1}$$

$$W \cos \theta + Z = m(\dot{w} - qu) \tag{2.2}$$

$$M = I_y \dot{q} \tag{2.3}$$

$$\dot{\theta} = q \tag{2.4}$$

$$\Delta\dot{h} = u \sin \theta - w \cos \theta \tag{2.5}$$

The quantity Δh represents the altitude variation measured during nonsteady maneuvering flight relative to the initial test flight altitude. Introducing the specific aerodynamic forces:

$$A_x \triangleq X/m = C_X \tfrac{1}{2}\rho V^2 S/m \tag{2.6}$$

and

$$A_z \triangleq Z/m = C_Z \tfrac{1}{2}\rho V^2 S/m \tag{2.7}$$

Eqs. (2.1) through (2.5) may be reduced and rearranged to yield the following set of simultaneous, first order, nonlinear kinematic relations:

$$\dot{u} = A_x - g \sin \theta - qw \tag{2.8}$$

$$\dot{w} = A_z + g \cos \theta + qu \tag{2.9}$$

$$\dot{\theta} = q \tag{2.10}$$

$$\Delta\dot{h} = u \sin \theta - w \cos \theta \tag{2.11}$$

Equation (2.3) can be omitted if q(t) is known (measured).

To set the stage for application of the Kalman filter and Kalman fixed interval smoothing algorithm to flight path estimation from onboard measurements, the time-dependent aircraft state variables u(t), w(t), θ(t) and Δh(t) can be considered as components of a vector-valued variable $\underline{X}$(t), characterizing the state of a dynamic system:

$$\underline{X} \triangleq \text{col } [u, w, \theta, \Delta h] \tag{2.12}$$

The simultaneous differential equations, Eqs. (2.8) through (2.11), can consequently be considered as the constituent components of a vector differential equation representing the evolution of the system's state.

The quantities A_x, A_z and q are considered as the components of a vector-valued system input signal:

$$\underline{U} \triangleq \text{col } [A_x, A_z, q] \tag{2.13}$$

The state equation of the dynamic system considered may be symbolically represented by the following nonlinear vector differential equation:

$$\dot{\underline{X}} = \underline{f}(\underline{X}, \underline{U}, t) \tag{2.14}$$

The initial state is:

$$\underline{X}(t_o) = \underline{X}(0) \tag{2.15}$$

The accelerometer and rate gyroscope measurements of the input signal components, see Eq. (2.13), are assumed corrupted with constant bias "errors" $-\underline{\lambda}$ and zero mean, time-dependent random "errors" $-\underline{w}(t)$. The following linear "correction" model is defined to relate the "exact" magnitude of the input signal $\underline{U}(t)$ to the "uncorrected" measurements $\underline{U}_m(t)$ and the "corrections" $+\underline{\lambda}$ and $+\underline{w}(t)$ for the corresponding "errors" in the measurements:

$$\underline{U}(t) \triangleq \underline{U}_m(t) + \underline{\lambda} + \underline{w}(t) = \underline{U}^*(t) + \underline{\lambda} \tag{2.16}$$

where:

$$\underline{U}^*(t) \triangleq \underline{U}_m(t) + \underline{w}(t)^{**} \tag{2.17}$$

and

$$\underline{U}_m(t) \triangleq \text{col } [A_{x_m}(t), A_{z_m}(t), q_m(t)] \tag{2.18}$$

$$\underline{\lambda} \triangleq \text{col } [\lambda_x, \lambda_z, \lambda_q] \tag{2.19}$$

* Coreolis- and centrifugal forces as well as aeroelastic effects are neglected. Strictly speaking, the equations of motion used for dynamic system model design are therefore valid only for small low speed aircraft such as the DHC-2 Beaver test aircraft.

** The quantity $\underline{U}^*(t)$ is introduced only to simplify mathematical notations.

$$\underline{w}(t) \triangleq \text{col}\,[w_x(t),\ w_z(t),\ w_q(t)] \qquad (2.20)$$

The bias error corrections are assumed constant. Hence:

$$\dot{\underline{\lambda}} = 0 \qquad (2.21)$$

The random error corrections $\underline{w}(t)$ are considered as a vector-valued Gaussian white noise process with mean:

$$E[\underline{w}(t)] = 0 \qquad \text{for } \forall\ t \qquad (2.22)$$

and covariance:

$$E[\underline{w}(t)\underline{w}^T(t)] = W(t)\delta(t-\tau) \qquad \text{for } \forall\ t,\tau \qquad (2.23)$$

Substitution of Eq. (2.16) in Eq. (2.14) yields:

$$\dot{\underline{X}}(t) = \underline{f}'(\underline{X}(t),\ \underline{U}^*(t),\ \underline{\lambda}) \qquad (2.24)$$

Estimating the systems's state vector trajectory $\underline{X}(t)$, the Kalman filter may be thought of as attenuating the effects of the input signal perturbations $-\underline{w}(t)$ on the estimate $\hat{\underline{X}}(t)$.
The effects of the constant bias errors $-\underline{\lambda}$ on the state vector estimate $\underline{X}(t)$ are reduced by estimating the corrections $+\underline{\lambda}$ simultaneously with $\underline{X}(t)$. To estimate the corrections $+\underline{\lambda}$ with the Kalman estimation procedure, the parameters λ_x, λ_z and λ_q should be modelled as state vector components of a so called augmented system.

Defining the augmented state vector:

$$\underline{Y} \triangleq \text{col}\,[u,\ w,\ \theta,\ \Delta h,\ \lambda_x,\ \lambda_z,\ \lambda_q] \qquad (2.25)$$

and combining Eqs. (2.21) and (2.24) the following augmented system state equation can be formulated, writing:

$$\dot{\underline{Y}} = \underline{f}'(\underline{Y}(t),\ \underline{U}^*(t)) \qquad (2.26)$$

with initial condition:

$$\underline{Y}(t_o) = \underline{Y}(0) \qquad (2.27)$$

Quantities observed in flight as system output signals, in addition to the measured input signals A_{x_m}, A_{z_m} and q_m are the airspeed V and the altitude variation Δh. The rationale underlying this choice of output signals is the fact that these quantities are related algebraicly (i.e. memoryless) to the components u(t), w(t) and $\Delta h(t)$ of the system state vector, see Eq. (2.12), and characterize the aircraft's flight path relative to the surrounding air mass, assumed at rest relative to the earth and provided that no static pressure gradients are traversed. Moreover, these quantities are easily measured with barometric sensors.

The output signals selected are by definition the components of the vector-valued output signal $\underline{M}(t)$:

$$\underline{M} \triangleq \text{col}\,[V,\ \Delta h] = \text{col}\,[\sqrt{u^2 + w^2},\ \Delta h] \qquad (2.28)$$

which is symbolically represented by the observation equation:

$$\underline{M} = \underline{h}(\underline{Y}) \qquad (2.29)$$

The output signal measurements $\underline{M}_m(t)$ are assumed to be corrupted with random measurement errors $-\underline{g}(t)$:

$$\underline{M}_m(t) \triangleq \text{col}\,[V_m(t),\ \Delta h_m(t)] = \\ = \underline{M}(t) - \underline{g}(t) = \underline{h}(\underline{Y}(t)) - \underline{g}(t) \qquad (2.30)$$

The random errors:

$$-\underline{g} \triangleq \text{col}\,[-q_V,\ -q_{\Delta h}] \qquad (2.31)$$

are considered as a vector-valued, Gaussian white noise process with mean:

$$E[\underline{g}(t)] = 0 \qquad \text{for } \forall\ t \qquad (2.32)$$

and covariance:

$$E[\underline{g}(t)\ \underline{g}^T(\tau)] = Q(t)\delta(t-\tau) \qquad \text{for } \forall\ t,\tau \qquad (2.33)$$

It is emphasized that no bias errors are included in the model for the output signal measurements, because of the fact that the barometric measurements of the airspeed V and the altitude variation Δh can be corrected for bias errors, prior to initiation of the estimation procedure. These errors are determined in flight, by shortcircuiting the pneumatic circuits of the corresponding transducers, prior to and after each test flight maneuver.

Linearization and discretization of the system model. The linear Kalman estimation procedure including the extended Kalman filter and extended Kalman fixed interval smoothing algorithm, (10,13,16,17), requires the system state equation, Eq. (2.26), and the observation equation, Eq. (2.30), to be linearized relative to a nominal state vector trajectory $\underline{Y}_{nom}(t)$ computed according to:

$$\underline{Y}_{nom}(t) = \underline{Y}_{nom}(0) + \int_0^t \underline{f}'(\underline{Y}_{nom}(\tau),\ \underline{U}^*_{nom}(\tau))d\tau \qquad (2.34)$$

where:

$$\underline{U}^*_{nom}(t) \triangleq \underline{U}_m(t) \qquad (2.35)$$

and

$$\underline{M}_{nom}(t) \triangleq \underline{h}(\underline{Y}_{nom}(t)) \qquad (2.36)$$

The Kalman estimation procedure is then used for estimation of state perturbation corrections:

$$\underline{y} \triangleq \underline{Y} - \underline{Y}_{nom} \qquad (2.37)$$

The estimated corrections $\hat{\underline{y}}$ are used to obtain state vector estimates $\hat{\underline{Y}}$ according to:

$$\hat{\underline{Y}} = \underline{Y}_{nom} + \hat{\underline{y}} \qquad (2.38)$$

Taking account of signal sampling, as performed by the flight test instrumentation system, the linearized state- and observation equations, Eqs. (2.26) and (2.30), are discretized for formulation of the discrete-time version of the Kalman estimation procedure.

A survey of the flight path reconstruction procedure is presented in the following block diagram, Fig. 2.2.

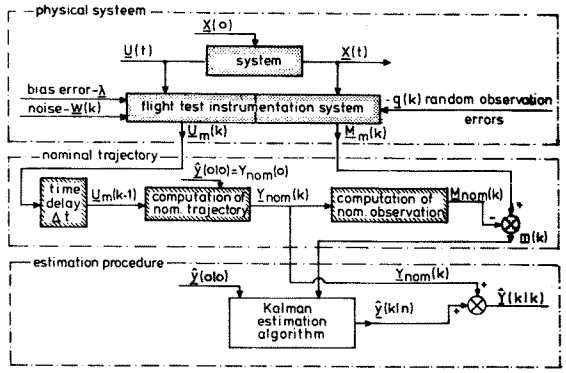

FIG 2.2: BLOCK DIAGRAM OF THE ENTIRE FLIGHT PATH RECONSTRUCTION PROCEDURE

Processing the flight test measurements A_{x_m}, A_{z_m}, q_m, V_m and Δh_m with the Kalman estimation procedure, finally yields estimated time histories of the system state variables u(t), w(t), θ(t), Δh(t) and estimates of the bias error corrections λ_x, λ_z and λ_q. Estimated time histories of the aircraft's airspeed V_a and the airflow angle of attack α_a can be computed from the estimated state variable time histories. In addition the Kalman estimation procedure derives an estimate of the covariance matrix $P(k|n)$ of the estimation errors $\hat{\underline{Y}}(k|n) - \underline{Y}(k)$, for k = 1,2,...,n, from all measurements available up to and including t_n.

Remark. The airspeed V_a and the airflow angle of attack α_a are most relevant in aircraft aerodynamics. Identification of the aircraft's aerodynamic model as well as derivation of aircraft performance data from flight test measurements in nonsteady flight therefore requires most accurate estimation of these quantities. In partieular accurate estimation of the angle of attack from the available inertial and barometric measurements, avoiding the problems involved in direct measurement with a boom mounted vane, is most relevant to successful application of the nonsteady flight test technique under consideration. Degradations in the accuracy of the estimated airspeed and angle of attack, resulting from steady and nonsteady atmospheric motions should in this respect be carefully evaluated.

2.1 Effects of atmospheric perturbations

Introduction. Hitherto it was assumed that flight tests are performed, flying through an airmass at rest over a flat, non rotating earth. According to this assumption all quantities measured with the inertial and barometric sensors mentioned may be defined just as well with respect to an earth-fixed reference frame F_e as to a reference frame F_a, attached to the airmass surrounding the aircraft. The following equalities hold in this case:

$$\underline{V}_{e_r}(t) = \underline{V}_{a_r}(t) \tag{2.39}$$

$$\alpha_{e_r}(t) = \alpha_{a_r}(t) \tag{2.40}$$

where $\underline{V}_{e_r}(t)$ and $\underline{V}_{a_r}(t)$ represent the velocity of the aircraft's c.g. respectively measured relative to F_e and F_a. The angles of attack $\alpha_{e_r}(t)$ and $\alpha_{a_r}(t)$ respectively are the angles enclosed between $\underline{V}_{e_r}$ and $\underline{V}_{a_r}$ and the X_b-axis of the aircraft's body frame of reference F_b. The suffix 'r' indicates flight through an airmass at rest; see for strictly symmetric flight Fig. 2.3.

The dynamic system model representing symmetric flight, see Eqs. (2.8) through (2.11), as well as the procedure developed for computation of an estimate $\hat{\underline{Y}}(0|0)$ (= $\underline{Y}_{nom}(0)$) of the initial state $\underline{Y}(0)$, see Eq. (2.34), are subject to these assumptions.

Effects of steady atmospheric motion. When flying under constant wind conditions, i.e. when F_a translates with a constant velocity:

$$\underline{V}_w \triangleq \text{col}\,[u_{we}, v_{we}, w_{we}] \tag{2.41}$$

relative to F_e, the following relations can be formulated using the subscript 'w' to indicate constant wind conditions:

$$\underline{V}_{e_w}(t) = \underline{V}_{e_r}(t) + \underline{V}_w \tag{2.42}$$

$$\underline{V}_{a_w}(t) = \underline{V}_{e_w}(t) - \underline{V}_w = \underline{V}_{e_r}(t) = \underline{V}_{a_r}(t) \tag{2.43}$$

see Eq. (2.39).

Since the aircraft's aerodynamics are invariant under constant translation of F_a relative to F_e, or equivalently of F_e relative to F_a, the angle of pitch will not be affected by constant wind. Hence:

$$\theta_{e_w}(t) = \theta_{e_r}(t) \tag{2.44}$$

From Eqs. (2.43) and (2.44) it follows that:

$$\alpha_{a_w} = \alpha_{a_r} \tag{2.45}$$

However, the flight path angle is affected according to:

$$\gamma_{e_w} - \gamma_{e_r} \approx C_{e_w}/V_{e_w} - C_{e_r}/V_{e_r} \approx w_{we}/V_m \tag{2.46}$$

see Fig. 2.3, and since α(t) is estimated using the relation:

$$\alpha_e(t) = \theta_e(t) - \gamma_e(t) \tag{2.47}$$

it can be concluded that:

$$\alpha_{e_w} - \alpha_{e_r} = \alpha_{e_w} - \alpha_{a_r} = \theta_{e_w} - \gamma_{e_w} - \theta_{e_r} + \gamma_{e_r} \approx -w_{we}/V_m \tag{2.48}$$

see Eq. (2.44), which implies that the angle of attack $\hat{\alpha}_{e_w}$, estimated under constant wind conditions, will differ from the actual airflow angle of attack $\alpha_{a_r}(t)$ under static atmospheric conditions by an amount:

$$\alpha_{w_{we}} \approx -w_{we}/V_m \tag{2.49}$$

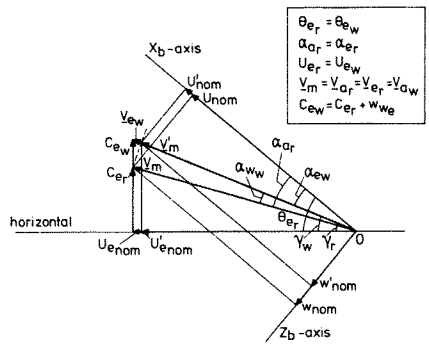

FIG 2.3: EFFECTS OF CONSTANT VERTICAL WIND ON THE ESTIMATED ANGLE OF ATTACK.

When flying through a constant horizontal static pressure gradient the estimated angle of attack will again be biased relative to the actual airflow angle of attack, since the effects of such gradients on the barometric measurements Δh_m, and consequently on the flight path angle $\hat{\gamma}$, estimated using the measurements $\Delta h_m(k)$ are similar to those of a constant rate of climb increment ΔC_e as resulting from constant vertical wind w_{we}, see Fig. 2.3. Traversing a constant wind speed gradient during flight testing should be expected to affect the estimates of the bias error corrections, as the Kalman filter may be thought of to compare the airspeed computed by simultaneous integration of Eqs. (2.8) through (2.10) with the airspeed observed, see Eq. (2.28), for estimation of the system state $\underline{Y}$. The probability of encountering static pressure and airspeed gradients obviously increases with increasing distance traversed during a single maneuver. From Eq. (2.49) it follows that the effect of constant vertical wind on the deviations of $\hat{\alpha}_{e_w}$ from α_{a_r} decreases with increasing airspeed.
The estimated quantity $\hat{V}_{e_w}(t)$ is unaffected by the horizontal component of constant wind $\hat{V}_w$, since estimation of the airspeed V depends mainly on the measurements $\underline{U}_m$ and V_m which are insensitive to constant wind, see Eqs. (2.43) and (2.45).

Effects of nonsteady atmospheric motion. If the aircraft flies through an airmass in nonsteady motion, i.e. in atmospheric turbulence, the following relations hold:

$$\underline{V}_{a_t}(t) = \underline{V}_{e_t}(t) - \underline{V}_g(t) \qquad (2.50)$$

and

$$\alpha_{a_t}(t) = \alpha_{e_t}(t) + \alpha_g(t) \qquad (2.51)$$

The subscript 't' is used to indicate flight in turbulence and $\underline{V}_g$ represents the gust verlocity vector of F_a measured relative to F_e:

$$\underline{V}_g(t) \triangleq \text{col}\,[u_{gs}(t),\ v_{gs}(t),\ w_{gs}(t)] \qquad (2.52)$$

The quantities u_{gs}, v_{gs} and w_{gs} are the components of $\underline{V}_g$ parallel to and positive in the negative directions of the X_s-, Y_s- and Z_s-axes of the stability frame F_s, see Fig. 2.4 for symmetric gusts, i.e. $v_{gs} = 0$.

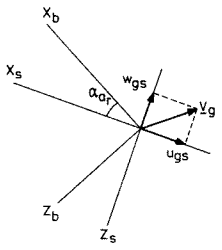

FIG. 2.4: THE COMPONENTS OF $\underline{V}_g$ DEFINED RELATIVE TO THE STABILITY FRAME F_s

Since the airspeed as well as the airflow angle of attack are affected by atmospheric turbulence, all aerodynamic quantities of interest and consequently all variables measured will be affected as well. The effects are dependent on aircraft characteristics and flight regime.

The deviation of $\hat{\alpha}_{e_t}$ from α_{a_r} can be shown to depend on the airspeed V and several aerodynamic derivatives as well as the relative aircraft mass μ_c. The deviation of the airspeed $\hat{V}_{e_t}(t)$ estimated under conditions of atmospheric turbulence from the actual airspeed $V_{a_r}(t)$ under static atmospheric conditions depends again on the aircraft's dynamic response characteristics [10,15].

2.2 Aerodynamic model identification

The aerodynamic model. Once the flight path reconstruction results required have been obtained further analysis is directed towards the identification of the mathematical model for the aircraft's aerodynamics. Obviously the complexity of a model representing the aerodynamic characteristics of an aircraft depends on the class and type of aircraft under consideration, on the section of the aircraft's flight envelope and the response frequency ranges to be covered. In this paper attention is focussed first of all on the identification of a model representing the aerodynamics of a small rigid low subsonic, propeller driven aircraft in nominally symmetric flight (in the flaps-up condition), and secondly on the identification of an aerodynamic model of a rigid, transonic, jet aircraft in nominally symmetric nonsteady maneuvering flight. The models are supposed to be valid throughout a considerable section of the aircraft's flight envelope. The aerodynamic model of the subsonic, propeller driven aircraft includes a relation between the dimensionless pressure increase measured in the propeller slipstream $\Delta p_t/\frac{1}{2}\rho V^2$ and the engine power P which is in its turn computed, using the engine power chart provided by the engine manufacturer, from manifold pressure and engine speed settings recorded in flight.
Since the input axes of the accelerometers and rate gyroscope included in the flight test instrumentation system are aligned along the aircraft's body axes, these axes are used for aerodynamic model formulation. In [3,6,7] the following aerodynamic model equations have been formulated and motivated:

$$C_X = C_{X_o} + C_{X_{\Delta p_t}}(\Delta p_t/\tfrac{1}{2}\rho V^2) + C_{X_\alpha}\alpha + C_{X_{\alpha^2}}\alpha^2 \qquad (2.53)$$

$$C_Z = C_{Z_o} + C_{Z_{\Delta p_t}}(\Delta p_t/\tfrac{1}{2}\rho V^2) + C_{Z_\alpha}\alpha + C_{Z_q}(q\bar{c}/V) + C_{Z_\delta}\delta_e \qquad (2.54)$$

$$C_m = C_{m_o} + C_{m_{\Delta p_t}}(\Delta p_t/\tfrac{1}{2}\rho V^2) + C_{m_\alpha}\alpha + C_{m_{\alpha^2}}\alpha^2 + C_{m_q}(q\bar{c}/V) + C_{m_\delta}\delta_e \qquad (2.55)$$

$$\Delta p_t/\tfrac{1}{2}\rho V^2 = a + b(P/\tfrac{1}{2}\rho V^3) + c(P/\tfrac{1}{2}\rho V^3)^2 \qquad (2.56)$$

The formulation of these equations is based in principle on the relations:

$$C_X = T_c \cos\alpha_T + C_L \sin\alpha - C_D \cos\alpha \qquad (2.57)$$

$$C_Z = -T_c \sin\alpha_T - C_L \cos\alpha - C_D \sin\alpha + C_{Z_\delta}\delta_e \qquad (2.58)$$

and

$$C_m = C_{m_o} + C_{m_{T_c}} T_c + C_{m_\alpha}\alpha + C_{m_\delta}\delta_e \qquad (2.59)$$

completed with terms depending on $q\bar{c}/V$ and $\dot{\alpha}\bar{c}/V$ to represent the effects of symmetric nonsteady motions

of the aircraft on the aerodynamic forces and moments X, Z and M.
Substitution of the thrust coefficient T_c by $\Delta p_t/\frac{1}{2}\rho V^2 S$ is based on the linear relationship between T_c and $\Delta p_t/\frac{1}{2}\rho V^2 S$ which follows from aerodynamic theory and which has been verified by means of wind tunnel experiments.
The linear expression for the lift curve:

$$C_L = C_{L_\alpha} (\alpha - \alpha_o) \tag{2.60}$$

and the quadratic expression for the polar drag curve:

$$C_D = C_{D_o} + (1/\pi Ae) (C_L - C_{L_1})^2 \tag{2.61}$$

are used to obtain the final expressions for Eqs. (2.53) and (2.54). Moreover the terms governing the dependence of the aerodynamic coefficient C_X on the variables $\dot{\alpha}\bar{c}/V$ and $q\bar{c}/V$ are assumed negligibly small for the aircraft under consideration.

The terms $C_{Z_q}(q\bar{c}/V)$ and $C_{m_q}(q\bar{c}/V)$ in Eqs. (2.54) and (2.55) represent both the contributions of $\dot{\alpha}\bar{c}/V$ and $q\bar{c}/V$ respectively to C_Z and C_m because of the linear relation between these two variables, apparent from the linear small-perturbation equations of aircraft motion [7].

Principles underlying aerodynamic model identification. The extraction of the aerodynamic model from nonsteady maneuvering flight test data is based mainly on three principles. First of all the aerodynamic model structure should be very roughly known* prior to estimation of model parameters from test flight data. Secondly the shape and structure of the nonsteady flight test maneuver should be selected such that the aircraft traverses the flight envelope of interest in the course of a single maneuver. In addition the maneuver should be shaped so as to optimize the identifiability of aerodynamic model parameters, i.e. to achieve maximal accuracy when extracting the aerodynamic model from the measurements obtained.
The third principle underlying aerodynamic model extraction from nonsteady maneuvering test flights is the property of the inertial accelerometers to directly measure the external aerodynamic forces acting on the aircraft. In particular measurement of the specific aerodynamic forces A_x and A_z with aircraft body-fixed accelerometers is based on this property.

In the context of this study regression analysis is used to extract the parameters in Eqs. (2.53) through (2.56) from flight test data [10,19-21].

3. Determination of aircraft steady flight characteristics from nonsteady maneuvering flight test data

3.0 Introduction

As already stated in Section 1, the aircraft's steady flight characteristics can be calculated from the aerodynamic model identified as well as estimated directly from the flight path reconstruction results.

Deviations of the calculated characteristics from estimated data should be considered as relevant information for assessment of the suitability of the aerodynamic model identified for accurate calculation of the test aircraft characteristics, throughout the flight envelope traversed during flight testing.

In what follows the suffix '1' will be used to indicate variable magnitudes characterizing nonsteady flight conditions, whereas the suffix '2' will be used to indicate variable magnitudes characterizing steady flight conditions.

3.1 Calculation and estimation of aircraft characteristics

Introduction. Calculation of aircraft performance, stability and control characteristic data points from aerodynamic model data as well as estimation of these characteristic data points by correction of quasi-steady to steady flight conditions is based in principle on iteratively solving Eqs. (2.1) through (2.3), (2.53) through (2.56), and the transformation relations:

$$\tan \alpha = w/u \tag{3.1}$$

$$V = \sqrt{u^2 + w^2} \tag{3.2}$$

to respectively obtain the magnitudes C_{X_2}, C_{Z_2}, C_{m_2}, u_2, w_2, θ_2, q_2, α_2, V_2, $(\Delta p_t/\frac{1}{2}\rho V^2)_2$ and δ_{e_2} characterizing steady flight or the corresponding corrections from quasi-steady or nonsteady to steady flight conditions:

$$\Delta C_X \triangleq C_{X_2} - C_{X_1} \tag{3.3}$$

$$\Delta C_Z \triangleq C_{Z_2} - C_{Z_1} \tag{3.4}$$

$$\vdots$$

$$\Delta (\Delta p_t/\tfrac{1}{2}\rho V^2) \triangleq (\Delta p_t/\tfrac{1}{2}\rho V^2)_2 - (\Delta p_t/\tfrac{1}{2}\rho V^2)_1 \tag{3.5}$$

$$\Delta\delta_e \triangleq \delta_{e_2} - \delta_{e_1} \tag{3.6}$$

under standardized aircraft and atmospheric conditions specified in terms of aircraft weight W_2, aircraft centre of gravity location $x_{c.g.2}$ and $z_{c.g.2}$, engine power P_2 and air density ρ_2 (corresponding with standard static pressure and air temperature), taking account of prespecified magnitudes or relations for two out of the eleven variables listed above. The aircraft characteristics to be computed are determined in fact by means of the additional relations specified. Calculation of the polar drag curve and lift curve can alternatively be achieved by direct computation of the key parameters C_{D_o}, C_{L_1}, e, C_{L_α} and α_o, see Eqs. (2.57), (2.58), (2.60) and (2.61), from the aerodynamic model coefficients, see Eqs. (2.53), (2.54) and (2.56), [3,10].

Calculation of aircraft characteristics from aerodynamic model data. Calculation of performance, stability and control characteristics in steady rectilinear flight is achieved iteratively solving Eqs. (2.1) through (2.3), (2.53) through (2.56), (3.1) and (3.2) under the conditions:

$$\dot{u}_2 = \dot{w}_2 = \dot{q}_2 = q_2 = 0 \tag{3.7}$$

for given aerodynamic model parameter magnitudes, see Eqs. (2.53) through (2.56), and either angle of

* A priori knowledge of the aerodynamic model can be deduced from theoretical analysis or wind tunnel experiments.

attack α_2 or airspeed V_2. If so desired, calculation of aircraft maneuvering characteristics in the point of horizontal flight of a steady pull-up maneuver may be obtained by solving the same equations under the conditions:

$$\dot{u}_2 = \dot{w}_2 = \dot{q}_2 = 0 \tag{3.8}$$

for given aerodynamic model data, α_2 and V_2 and centre of gravity location $x_{c.g.2}$ and $z_{c.g.2}$ and setting:

$$\theta_2 = \alpha_2 \tag{3.9}$$

The accuracy of aircraft characteristics calculated from aerodynamic model data obviously depends entirely on the accuracy of the aerodynamic model identified. More precisely the achievable accuracy depends on the suitability of the model extracted from nonsteady maneuvering flight measurements, to accurately represent the aircraft's aerodynamics throughout the flight envelope traversed during flight testing.

Estimation of aircraft characteristics from flight test data. Correction from quasi-steady flight to steady flight conditions is achieved by solving the same set of equations, Eqs. (2.1) through (2.3), (2.53) through (2.56), (3.1) and (3.2), to obtain the correction magnitudes, ΔC_X, ΔC_Z, ..., $\Delta(\Delta p_t/\frac{1}{2}\rho V^2)$ and $\Delta\delta_e$, see Eqs. (3.3) through (3.6), under similar conditions as specified for the calculation of aircraft characteristics from aerodynamic model data and prespecifying either:

$$\Delta\alpha = \alpha_2 - \alpha_1 \tag{3.10}$$

or

$$\Delta V = V_2 - V_1 \tag{3.11}$$

or both, as well as using the magnitudes C_{X_1}, C_{Z_1}, C_{m_1}, $(\Delta p_t/\frac{1}{2}\rho V^2)_1$, V_1, α_1, θ_1, $(q\bar{c}/V)_1$ and δ_{e_1} derived from flight test measurements, the pertaining nonsteady test flight conditions W_1, P_1, ρ_1, $x_{c.g.1}$ and $z_{c.g.1}$, and the aerodynamic model parameters identified.

Correcting the aerodynamic coefficients C_{Z_1} and C_{m_1} to steady flight conditions with respect to a standard centre of gravity location the following relations should be used:

$$C_{Z_2} = C_{Z_o} + C_{Z_{\Delta p_t}}(\Delta p_t/\tfrac{1}{2}\rho V^2)_2 + C_{Z_\alpha}\alpha_2 + C^*_{Z_q}(q\bar{c}/V)_2 + C_{Z_\delta}\delta_{e_2} \tag{3.12}$$

and

$$C_{m_2} = C_{m_o} + C_{m_{\Delta p_t}}(\Delta p_t/\tfrac{1}{2}\rho V^2)_2 + C_{m_\alpha}\alpha_2 + C_{m_{\alpha^2}}\alpha_2^2 + C^*_{m_q}(q\bar{c}/V)_2 + C_{m_\delta}\delta_{e_2} - (\Delta x_{c.g.}/\bar{c})\,C_{Z_2} + (\Delta z_{c.g.}/\bar{c})\,C_{X_2} \tag{3.13}$$

where

$$C^*_{Z_q} = C_{Z_q} - (\Delta x_{c.g.}/\ell_h)\,C_{Z_q} \tag{3.14}$$

and

$$C^*_{m_q} = C_{m_q} - (\Delta x_{c.g.}/\bar{c})\,C_{Z_q} \tag{3.15}$$

if the pitch rate dependent contributions:

$$\Delta Z_q = \tfrac{1}{2}\rho V^2 S\, C_{Z_q} \tag{3.16}$$

and

$$\Delta M_q = \tfrac{1}{2}\rho V^2 S\bar{c}\, C_{m_q} \tag{3.17}$$

to the aerodynamic force Z and moment M, are generated mainly by the horizontal tailplane. Otherwise:

$$C^*_{Z_q} = C_{Z_q} - C_{Z_\alpha}(\Delta x_{c.g.}/\bar{c}) \tag{3.18}$$

and

$$C^*_{m_q} = C_{m_q} - C^*_{Z_q}(\Delta x_{c.g.}/\bar{c}) - C_{m_\alpha}(\Delta x_{c.g.}/\bar{c}) \tag{3.19}$$

Computing aircraft characteristics in steady rectilinear flight the following relations are most relevant:

1. the relation:

$$V_2^2 = W/(\tfrac{1}{2}\rho S\sqrt{C_{X_2}^2 + C_{Z_2}^2}) \tag{3.20}$$

which permits estimation of the airspeed V_2 taking account of the fact that the total aerodynamic force $C_R\frac{1}{2}\rho V_2^2 S$ on the aircraft balances aircraft weight in steady rectilinear flight.

2. the relation:

$$\theta_2 = -\arctan(C_{X_2}/C_{Z_2}) \tag{3.21}$$

which follows from Eqs. (2.1) and (2.2) when taking account of the conditions expressed by Eq. (3.7),

3. the relation:

$$C_2 = V_2 \sin(\theta_2 - \alpha_2) \tag{3.22}$$

permitting computation of the rate of climb, in steady rectilinear flight.

Provided that the quasi-steady flight conditions observed closely approximate steady flight conditions the accuracy of aircraft characteristics obtained by correcting quasi-steady or nonsteady flight conditions towards steady flight conditions depends to a major extent on the accuracy of nonsteady flight data such as for example the flight path reconstruction results, $\hat{V}$, $\hat{\alpha}$ and $\hat{\theta}$, estimated from flight test measurements. More detailed information concerning the methods applied to correct nonsteady flight test data to steady flight conditions will be published in [11].

4. Results obtained from flight testing a low speed, propeller driven aircraft

4.0 Introduction

The aircraft steady flight characteristics, in this section as an illustration of the preceding theoretical concepts derived from nominally symmetric nonsteady maneuvering flight test data, are the polar drag curve, the lift curve and the curves representing rate of climb and elevator angle to trim as a function of airspeed in steady straight flight. Results obtained from flight testing a high wing, light weight, single engined, propeller driven, low

subsonic aircraft will be presented and discussed in this section. The aircraft flight tested was the De Havilland DHC-2 Beaver aircraft, owned and operated by the Delft University of Technology.

In addition to processing actual onboard measurements, digitally simulated test flight data [10] have been analysed for detailed investigations into the effects of measurement errors and atmospheric perturbations on the accuracy of steady flight characteristics derived from nonsteady maneuvering test flights. The accuracy* of the characteristics derived from digitally simulated flight test measurements as well as the precision** of similar data derived from actual onboard measurements should be considered as stringent criteria for validation of the performance of the entire estimation procedure including flight path reconstruction and aerodynamic model identification. The precision of a sample of N similar characteristics corresponding to N nonsteady maneuvering flight tests, i.e. the scatter of these characteristics relative to the sample mean, should be understood to convey information on the reproducibility of the experimental results obtained, rather than on the accuracy of the sample mean.

4.1 The flight test instrumentation system

The flight test instrumentation system used included amongst others:

1. three Donner type 4310 force balance accelerometers for measurement of specific aerodynamic forces in m/s^2 with a resolution of 1 in 10^4,
2. a Nortronics type GI-H5-.5 rate gyroscope for measurement of the aircraft's rate of pitch in rad/s with a resolution better than 1 in 10^4,
3. S.E.L. 150 barometric sensors for measurement of airspeed and altitude variation, with an accuracy better than 0.25%,
4. a E.A.I. type 26.070 digital Volt-meter for sampling and digitizing transducer output voltages, range 0-10 V, accuracy 0.03%,
5. a parallel to series converter for serial recording of the sampled and digitized signals on a two-track magnetic tape.

Rms magnitudes of the random errors in the measurements of the inertial and barometric sensors as deduced from laboratory calibration results are listed in Table 4.1.

Table 4.1. Rms measurement error magnitudes

Rms measurement errors	Value	Unit
σ_{w_x}	0.4×10^{-2}	m/s^2
σ_{w_z}	0.4×10^{-2}	m/s^2
σ_{w_q}	0.15×10^{-3}	rad/s
σ_{q_V}	0.15	m/s
$\sigma_{q_{\Delta h}}$	0.2	m

4.2 The nonsteady maneuver

The nonsteady maneuver used for flight testing the DHC-2 Beaver aircraft can be described as follows. The aircraft is initially brought into a nearly steady condition at a low airspeed. A gradual, downward deflection of the elevator is commenced after a few seconds, resulting in an approximately 0.5 m/s^2 forward acceleration of the aircraft, see Fig. 4.1. The airspeed is increased from 35 m/s up to approximately 65 m/s.

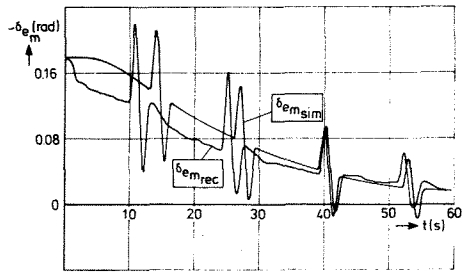

FIG. 4.1: SIMULATED AND ACTUALLY RECORDED TIME HISTORY $\delta_{e_m}(t)$

The gradual downward deflection of the elevator is interrupted at four instants, approximately equally spaced in time, to perform a short pull-up push-down oscillation. The flight conditions between the oscillations performed, see Fig. 4.1, can to a certain extent be considered as quasi-steady [7]. During the oscillations the aircraft's motions should be considered as highly nonsteady.
Considerable normal accelerations and rotation rates then occur. During nonsteady maneuvering flight the normal load factor varies from 0.6 up to 1.4.

4.3 Experimental results

Results obtained by processing actual onboard measurements. The results obtained by analysing ten flight test maneuvers FT1 through FT10 are listed below. First of all to characterize flight path reconstruction results, estimates of the inertial bias error corrections $\underline{\lambda}$, see Eqs. (2.16) and (2.19), as well as mean and rms magnitudes of the flight path reconstruction residuals defined according to:

$$\Delta V_r \triangleq V_m - \hat{V}(k|n) \tag{4.1}$$

and

$$\Delta\Delta h_r \triangleq \Delta h_m - \hat{\Delta h}(k|n) \tag{4.2}$$

as obtained after processing all available measurements with the Kalman estimation procedure, are listed in Tables 4.2 and 4.3.

Comparing the estimates of the bias error corrections listed in Table 4.2 to the rms estimation error magnitudes as generated by the extended Kalman filter procedure after processing n measurements it may be concluded that the corrections λ_z and λ_q can

* Accuracy is a measure of how close the outcome of a measurement, or a sequence of observations approaches the true value of a specified parameter [22].

** Precision is a measure of how close the outcome of a measurement, or a sequence of observations, clusters about some estimated value of a specified parameter [22].

Table 4.2. Bias error corrections estimated from 10 flight test maneuvers FT1 through FT10

Flight test maneuver	$\hat{\lambda}_x(n\|n)$ (m/s^2)	$\sigma_{\hat{\lambda}_x}(n\|n)$ (m/s^2)	$\hat{\lambda}_z(n\|n)$ (m/s^2)	$\sigma_{\hat{\lambda}_z}(n\|n)$ (m/s^2)	$\hat{\lambda}_q(n\|n)$ (rad/s)	$\sigma_{\hat{\lambda}_q}(n\|n)$ (rad/s)
FT1	0.0321	0.0040	0.0029	0.0006	-0.0001	0.0001
FT2	-0.0162	0.0029	-0.0071	0.0006	-0.0004	0.0001
FT3	-0.0231	0.0036	-0.0061	0.0006	-0.0002	0.0001
FT4	-0.0024	0.0037	0.0070	0.0006	-0.0002	0.0001
FT5	-0.0366	0.0035	0.0010	0.0005	-0.0001	0.0001
FT6	-0.0305	0.0027	-0.0006	0.0005	-0.0003	0.0001
FT7	-0.0079	0.0036	0.0010	0.0006	-0.0004	0.0001
FT8	-0.0174	0.0039	-0.0056	0.0007	-0.0002	0.0001
FT9	-0.0282	0.0048	-0.0028	0.0007	-0.0003	0.0001
FT10	-0.0383	0.0039	-0.0023	0.0007	-0.0002	0.0001

Table 4.3 Mean and rms magnitudes of flight path reconstruction residuals from ten flight test maneuvers FT1 through FT10

Flight test maneuver	$\overline{\Delta V}_r$ (m/s)	$\sigma_{\Delta V_r}$ (m/s)	$\overline{\Delta\Delta h}_r$ (m)	$\sigma_{\Delta\Delta h_r}$ (m)
FT1	-0.0025	0.1156	0.0002	0.1640
FT2	0.0054	0.1131	-0.0002	0.1958
FT3	-0.0047	0.1125	0.0002	0.1745
FT4	-0.0068	0.1600	0.0001	0.1602
FT5	0.0027	0.0958	0.0003	0.1749
FT6	0.0034	0.0870	0.0001	0.1710
FT7	-0.0036	0.1162	0.0005	0.1566
FT8	-0.0031	0.1048	0.0000	0.1640
FT9	-0.0044	0.1320	0.0000	0.2030
FT10	-0.0025	0.1010	0.0001	0.2130

be estimated with sufficient accuracy such in contrast to the estimates of the bias error corrections λ_x, showing rms estimation error magnitudes greater than 10% of the magnitudes of the corresponding estimates. The estimates $\hat{\lambda}_x(n|n)$, $\hat{\lambda}_z(n|n)$ and $\hat{\lambda}_q(n|n)$ are unaffected when applying the Kalman fixed interval smoothing procedure posterior to filtering the n measurements available, (23).

Comparison of the data listed in Table 4.3 with the rms measurement errors specified in Table 4.1 shows the flight path reconstruction residuals obtained to have rms magnitudes equivalent to the corresponding rms errors σ_{q_V} and $\sigma_{q_{\Delta h}}$ respectively in the measurements V_m and Δh_m.

Aerodynamic model identification results obtained by processing flight test data of the 10 flight test maneuvers FT1 through FT10, are listed in Table 4.4 in terms of:

1. the sample means:

$$\bar{\hat{a}}_i = \frac{1}{10} \sum_{j=1}^{10} \hat{a}_{i,j}(n) \qquad (4.3)$$

of the ten estimates $\hat{a}_{i,j}(n)$, for j = 1,2,...,10, of the aerodynamic model parameters a_i, see Eqs. (2.53) through (2.56), extracted from the ten corresponding nonsteady maneuvering flight tests FT1 through FT10, by processing all measurements available per maneuver up to and including those recorded at maneuver completion time t_n,

2. the sample standard deviations:

$$s_{\hat{a}_i} = \sqrt{\frac{1}{9} \sum_{j=1}^{10} \{\hat{a}_{i,j}(n) - \bar{\hat{a}}_i\}^2} \qquad (4.4)$$

reflecting the scatter in (i.e. the repeatability of) the identification results,

3. the relative sample standard deviations:

$$s_{r_i} = (s_{\hat{a}_i}/\bar{\hat{a}}_i) \cdot 100\% \qquad (4.5)$$

Table 4.4. Aerodynamic model identification results obtained from ten flight test maneuvers FT1 through FT10

Parameter	$\bar{\hat{a}}_i$	$s_{\hat{a}_i}$	s_{r_i}(%)
C_{X_o}	- 0.0511	0.0027	5.28
$C_{X_{\Delta p_t}}$	0.1382	0.0056	4.05
C_{X_α}	0.2169	0.0610	28.12
$C_{X_{\alpha 2}}$	3.5321	0.2706	7.66
C_{Z_o}	- 0.1529	0.0347	22.69
$C_{Z_{\Delta p_t}}$	- 0.0232	0.0292	125.86
C_{Z_α}	- 5.6587	0.1443	2.55
C_{Z_q}	- 3.8705	0.5351	13.83
C_{Z_δ}	- 0.5848	0.0081	1.39
C_{m_o}	0.0182	0.0057	31.22
$C_{m_{\Delta p_t}}$	- 0.0240	0.0074	30.83
C_{m_α}	- 0.9879	0.0722	7.31
$C_{m_{\alpha 2}}$	- 1.6271	0.2004	12.32
C_{m_q}	-19.1850	0.4853	2.53
C_{m_δ}	- 2.2222	0.0308	1.39
a	0.0532	0.0078	14.66
b	16.2332	0.3395	2.09
c	-20.1769	1.5633	7.75

From Table 4.4 the coefficients C_{X_α}, C_{Z_0}, $C_{Z_{\Delta p_t}}$, C_{Z_q}, C_{m_o}, $C_{m_{\Delta p_t}}$, $C_{m_{\alpha 2}}$ and a should be noticed to be estimated with relative sample standard deviations greater than 10%. The most important coefficients $C_{X_{\Delta p_t}}$, $C_{X_{\alpha 2}}$, C_{Z_α}, C_{m_q}, C_{m_δ} and b may be seen to be estimated with relative sample standard deviations smaller than 10%.

The sample means of the aerodynamic model parameters have been used for correcting the aerodynamic forces X and Z, the aerodynamic moment M and the dimensionless propeller induced increase in total pressure $\Delta p_t/\frac{1}{2}\rho V^2$ measured in the quasi-steady parts of the flight test maneuvers to corresponding values related to exactly steady straight flight conditions and a set of "standard" values for engine rpm, manifold pressure, aircraft weight and centre of gravity, flight altitude and air temperature. In practice these corrections turn out

to be very small, such except for those corrections required for derivation of the polar drag curve from nonsteady flight test data. Identification errors in the aerodynamic model used for correction purposes, may in most cases consequently be assumed to have little effect on the steady state results obtained after correction. The accuracy of these results depends therefore to a considerable extent on flight path reconstruction accuracy.

The correction technique outlined in Section 3 may also be used to derive the polar drag curve and the lift curve from the quasi-steady and nonsteady intervals of the test flight maneuvers to be analysed. The zero power condition (i.e. $P_2 = 0$) specified for the polar drag curve and the lift curve, however, deviates considerably from engine power in nonsteady maneuvering flight (i.e. $P_1 \approx 275$ hp). Extrapolation from nonsteady conditions towards the steady flight conditions specified for these curves should be expected to yield less accurate results, as the large corrections required may be expected to be more sensitive to errors in the aerodynamic models identified.

Having reduced the magnitudes of C_{X_1} and C_{Z_1} to the corresponding zero-power steady state magnitudes C_{X_2} and C_{Z_2} taking account of the steady flight conditions specified for the polar drag curve and the lift curve, the corresponding data points C_L and C_D are computed according to:

$$C_L = C_{X_2} \sin \hat{\alpha}_2 - C_{Z_2} \cos \hat{\alpha}_2 \qquad (4.6)$$

$$C_D = - C_{X_2} \cos \hat{\alpha}_2 - C_{Z_2} \sin \hat{\alpha}_2 \qquad (4.7)$$

The accuracy of the $C_L - C_D$ data points obtained by transforming the C_{X_2}-C_{Z_2} data points will be limited by atmospheric perturbations since the transformation applied depends on the estimated angle of attack $\hat{\alpha}_2$ which has been shown to deviate from the airflow angle of attack α_a actually required as a result of constant wind and atmospheric turbulence.

Analysing the flight test maneuvers FT1 through FT10 according to Sections 2 and 3, and fitting curves through the performance, stability and control characteristic data points derived from each nonsteady maneuver, a sample of ten curves is obtained per aircraft characteristic of interest. The corresponding sample mean curves and the pertaining sample standard deviation curves are shown in Figs. 4.2 through 4.5, respectively for the aircraft's polar drag curve, the lift curve, the climb performance curve and the trim curve. Each figure shows in addition mean and sample standard deviation magnitudes of the pertaining data points calculated from the aerodynamic models identified, by processing the ten flight test maneuvers FT1 through FT10, see Section 3 and [3,10]. Studying Figs. 4.2 through 4.5 the polar drag curve, the lift curve and the climb performance curve should be observed to exhibit a significant scatter of the sample curves, whereas the trim curve exhibits a quite favourable precision. The polar drag curve seems to be the least accurate of the results presented. This could be expected from the remarks made concerning the absolute magnitude of the corrections to be made and the effects of atmospheric perturbations on the estimated angle of attack.

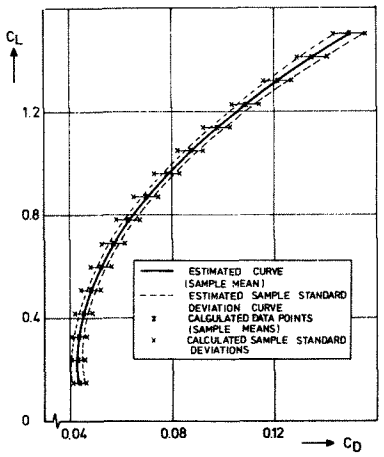

FIG. 4.2: POLAR DRAG CURVE; ACTUAL FLIGHT TEST MEASUREMENTS

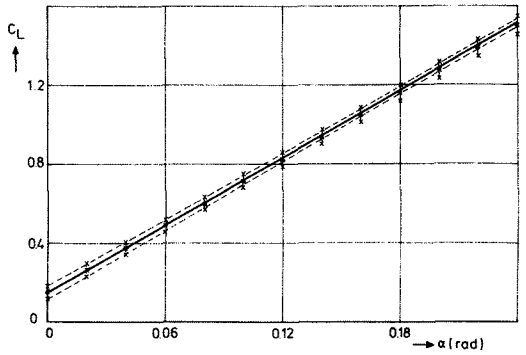

FIG. 4.3. LIFT CURVE; ACTUAL FLIGHT TEST MEASUREMENTS

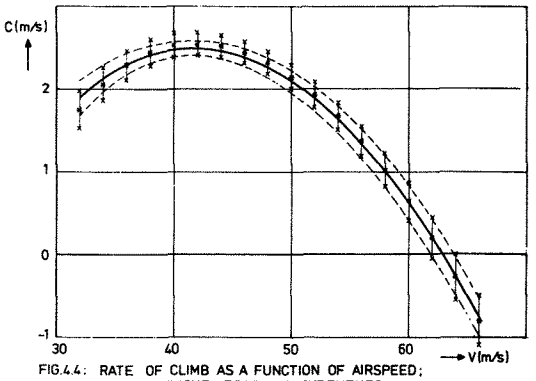

FIG. 4.4: RATE OF CLIMB AS A FUNCTION OF AIRSPEED; ACTUAL FLIGHT TEST MEASUREMENTS

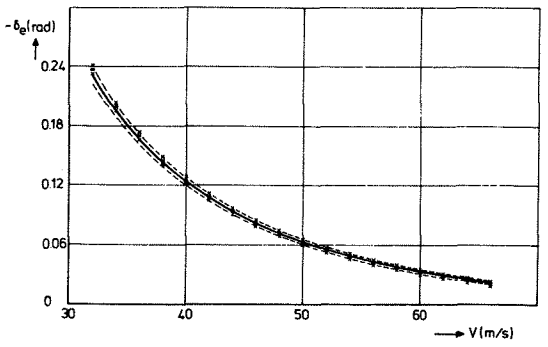

FIG. 4.5. TRIM CURVE; ACTUAL FLIGHT TEST MEASUREMENTS

Evidence for the statements made is to a certain extent provided by Fig. 4.6 combinedly showing the C_L-C_D-curve and the pertaining C_N-C_T-curve, both derived from the nonsteady flight test maneuvers FT1 through FT10.

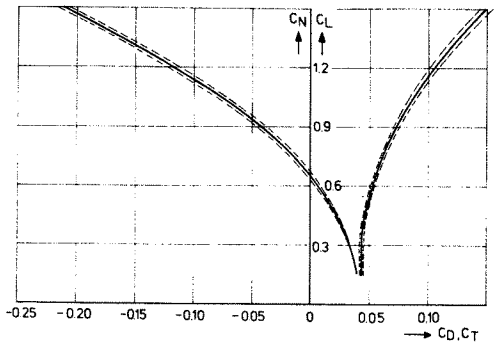

FIG.4.6: THE C_L-C_D CURVE AND THE CORRESPONDING C_N-C_T CURVE; ACTUAL FLIGHT TEST MEASUREMENTS

The computation of the C_N-C_T-curve does not involve the transformation equations, Eqs. (4.6) and (4.7), and the corresponding inaccuracies of $\hat{\alpha}_2$. The sample standard deviation of the C_N-C_T-curve may be seen to be a little smaller over the entire C_N-range as compared to the sample standard deviation of the C_L-C_D-curve shown over the entire C_L-range. Moreover it should be noticed that the sample standard deviation of the C_N-C_T-curve decreases with decreasing C_N as the sample standard deviation of the C_L-C_D-curve decreases with decreasing C_L. This phenomenon may be explained by the fact that the correction from actual flight conditions to the zero power condition, as specified for the C_L-C_D- and the C_N-C_T-curves both decrease in magnitude with increasing airspeed V. This results in a decreasing effect of thrust modelling errors, see Eq. (2.56), on the accuracy of both estimated characteristics.

Observing the sample means and sample standard deviations of the characteristic data points calculated directly from the aerodynamic model identification results, see Figs. 4.2 through 4.5, the accuracy of these data points may be concluded to be comparable in order of magnitude to the accuracy of the characteristics obtained by correcting nonsteady flight to steady flight conditions. This result provides evidence for the accuracy (reliability) of the aerodynamic model identified, see Table 4.4, throughout the flight envelope of interest.

Since the extrapolations from quasi-steady flight to steady flight conditions as required for calculation as well as estimation of rate of climb- and elevator angle to trim versus airspeed curves are small, the accuracy of these characteristics will be mainly limited by atmospheric perturbations rather than by aerodynamic model errors.

Results obtained by processing digitally simulated flight test measurements. To investigate whether either measurement errors or atmospheric perturbations are the most likely error sources in the computed polar drag curve and the C_N-C_T-curve, three simulation experiments, each comprising ten digitally simulated test flights, have been carried through. Results obtained by analysing actual test flight measurements should be noticed to differ in principle from those derived from digitally simulated test flight data as uncontrolable modelling errors can to a certain extent be avoided when performing simulation experiments.

The first set of ten digitally simulated test flights was used to experimentally verify the effects of measurement errors on the estimated characteristics discussed. The corresponding time history of the digitally simulated elevator angle measurement $\delta_{em_{sim}}(t)$ is shown in Fig. 4.1.
The second set was used to verify the effects of constant vertical wind on the estimated characteristics mentioned. The third set of ten digitally simulated test flights was used to verify the effects of low intensity atmospheric turbulence on the estimated aircraft characteristics. Measurement error statistics were set equal to laboratory calibration results. Constant vertical wind magnitudes were drawn from a normally distributed zero mean population with a standard deviation of:

$$\sigma_{w_{we}} = 0.20 \text{ m/s} \tag{4.8}$$

Simulated atmospheric turbulence was generated using the Dryden turbulence correlation models with standard deviations:

$$\sigma_{u_{gs}} = \sigma_{w_{gs}} = 0.20 \text{ m/s} \tag{4.9}$$

and scale length:

$$L_g = 300 \text{ m} \tag{4.10}$$

The aerodynamic models identified under the conditions of Exps. I, II and III are listed in Table 4.5 in terms of the sample means $\bar{\tilde{a}}_i$ and the relative sample standard deviations s_{r_i}, see Eqs. (4.3) and (4.5).

Sample means and sample standard deviations of data points of the corresponding polar drag curves and C_N-C_T-curves are listed in Table 4.6, in combination with the sample means and sample standard deviations of data points of similar curves estimated, see Fig. 4.6, from actual flight test measurements.

Studying the data listed in Table 4.6 the following conclusions may be drawn. Measurement errors as far as corresponding with laboratory calibration results may be seen to yield a scatter in the C_L-C_D- and C_N-C_T-curves less than 10 counts. Constant vertical wind in the order of 0.20 m/s results in a scatter in the C_L-C_D-curves varying from 2 to 82 counts, whereas the corresponding C_N-C_T-curves exhibit no scatter. The scatter in the C_L-C_D-curves obviously results from the effects of constant wind on $\hat{\alpha}$ and the subsequent transformations, Eqs. (4.6), and (4.7).
The atmospheric turbulence simulated resulted in a scatter varying from 20 to 60 counts in the C_L-C_D-curves and a scatter varying from 18 to 54 counts in the corresponding C_N-C_T-curves.
As the scatter in the C_N-C_T-curves is almost equivalent to the scatter in the C_L-C_D-curves, such in contrast to the results observed from the constant wind experiment, atmospheric turbulence should be concluded to result in gust modelling errors rather than transformation errors, affecting the C_N-C_T-curves and the C_L-C_D-curves, to an approximately similar extent.
From these experiments estimation of the C_L-C_D-curve may be expected to be more sensitive to atmospheric perturbations than estimation of the

Table 4.5. Aerodynamic model identification results obtained processing simulated flight test measurements from Exps. I, II and III

Parameter	$a_{i_{sim}}$	Exp. I		Exp. II		Exp. III	
		$\bar{\hat{a}}_i$	$s_{r_i}(\%)$	$\bar{\hat{a}}_i$	$s_{r_i}(\%)$	$\bar{\hat{a}}_i$	$s_{r_i}(\%)$
C_{X_o}	- 0.0511	- 0.0510	0.59	- 0.0514	0.07	- 0.0523	7.65
$C_{X_{\Delta p_t}}$	0.1382	0.1380	0.36	0.1390	1.37	0.1429	5.67
C_{X_α}	0.2169	0.2180	3.03	0.2148	6.94	0.1686	77.76
$C_{X_{\alpha 2}}$	3.5321	3.5297	0.69	3.5597	1.50	3.6589	14.58
C_{Z_o}	- 0.1457	- 0.1472	2.79	- 0.1428	9.10	- 0.1309	20.40
$C_{Z_{\Delta pt}}$	- 0.0234	- 0.0228	9.65	- 0.0280	36.79	- 0.0414	104.11
C_{Z_α}	- 5.6590	- 5.6580	0.09	- 5.6548	0.08	- 5.5388	3.63
C_{Z_q}	- 3.8985	- 3.8828	1.45	- 3.3902	2.02	- 3.9477	28.44
C_{Z_δ}	- 0.5871	- 0.5857	0.22	- 0.5839	0.04	- 0.5403	4.61
C_{m_o}	0.0350	0.0345	2.61	0.0352	6.25	0.0348	22.41
$C_{m_{\Delta p_t}}$	- 0.0238	- 0.0232	1.72	- 0.0239	11.30	- 0.0195	80.01
C_{m_α}	- 1.1506	- 1.1494	0.56	- 1.1471	0.95	- 1.0577	12.57
$C_{m_{\alpha 2}}$	- 1.5785	- 1.5844	1.35	- 1.5943	0.56	- 1.6778	33.13
C_{m_q}	-19.2074	-19.1327	0.25	-19.0625	0.08	-18.2901	7.21
C_{m_δ}	- 2.2309	- 2.2258	0.22	- 2.2190	0.04	- 2.0533	4.61
a	0.0532	0.0533	0.96	0.0526	0.01	0.0503	3.98
b	16.2332	16.2302	0.14	16.2643	0.00	16.3640	0.64
c	-20.1769	-20.1552	0.72	-20.4126	0.00	-21.0023	2.81

Table 4.6. Effects of modelling errors, measurement errors, and atmospheric perturbations on the accuracy of the estimated C_L-C_D- and C_N-C_T-curves

C_L, C_N	actual measurements		simulations					
			measurement errors		constant vertical wind		atmospheric turbulence $\sigma_{u_{gs}}=\sigma_{w_{gs}}=0.2$ m/s	
	C_D/σ_{C_D}	C_T/σ_{C_T}	C_D/σ_{C_D}	C_T/σ_{C_T}	C_D/σ_{C_D}	C_T/σ_{C_T}	C_D/σ_{C_D}	C_T/σ_{C_T}
0.15	429/25	396/8	437/3	436/4	437/2	444/0	444/60	484/33
0.60	525/19	56/15	517/1	38/3	521/21	36/0	557/20	41/18
1.05	880/25	- 780/26	870/2	- 807/6	869/48	- 816/0	913/43	- 834/39
1.50	1495/59	-2113/39	1496/9	-2099/8	1483/82	-2113/0	1511/57	-2143/54

The magnitudes of C_D, C_T, σ_{C_D} and σ_{C_T} are expressed in "drag counts", (1 drag count equals 0.0001).

C_N-C_T-curve. None of the simulation experiments revealed an exactly similar increase in accuracy (from 39 to 8 counts) of the C_N-C_T-curves with decreasing C_N as exhibited by the results derived from actual flight test measurements. In this context it should be noticed that thrust modelling (measurement) errors have not been simulated. The corresponding effects could therefore impossibly be verified. Wind tunnel experiments and further detailed thrust-drag flight test programs should provide further information on the effects of thrust modelling errors on the accuracy of performance characteristics estimated from nonsteady maneuvering flight test data.

5. Results obtained from flight testing a high subsonic jet aircraft

5.0 Introduction

Part of the experimental results obtained by flight testing the Hawker Hunter Mk VII jet aircraft, owned and operated by the National Aerospace Laboratory (NLR), are discussed in this section. Some data on this aircraft are listed in Table 5.1.

Table 5.1. Some data on the Hawker Hunter Mk VII

Length	14.90 m
Wing span	10.26 m
Wing surface	33.30 m^2
Wing sweep angle	40^o
Max. take off weight	9752 kg
Engine type	Rolls Royce Avon 122
Max. thrust at sea level	3450 kg

Evaluation of the applicability of the flight test method described in the previous sections to the class of high subsonic aircraft propelled by a straight jet engine has been the goal of the flight test program carried through. This program provides

a valuable extension of the flight test results obtained earlier, using the De Havilland DHC-2 Beaver, low speed, piston-engined aircraft.

First of all some remarks are made concerning the instrumentation system used. Secondly the shape of the nonsteady flight test maneuver performed is described. Finally some experimental results are presented and discussed.

5.1 The flight test instrumentation system

The instrumentation system used has been described in [25,26]. Nineteen inertial and barometric variables have been sampled and recorded at a rate of 20 samples per second and a resolution of 0.01%. Prior to, during and posterior to flight test program execution the complete instrumentation system was calibrated in the laboratory [25].

5.2 The nonsteady maneuver

The nominally symmetric nonsteady flight test maneuver remarkably resembles the maneuver used for flight testing the De Havilland DHC-2 Beaver aircraft, described in Section 4.
The maneuver is commenced at low speed, in approximately steady horizontal flight. Increase of thrust to a preselected level then results in a gradual acceleration of the aircraft.
Since the normal load factor approximately equals 1 and the rate of pitch q is close to zero the aircraft may be considered to be accelerating quasi-steadily from low speed to the speed compatible with the preselected engine thrust, nominal flight altitude and to the aircraft weight.

At various instants regularly spaced in time the quasi-steady motion is interrupted to perform non-steady pull-up push-down maneuvers.
Figure 5.1 presents a recorded time history of the elevator angle, typical for the nonsteady flight test maneuvers described above. The operational aspects of the execution of these maneuvers have been described in [24].

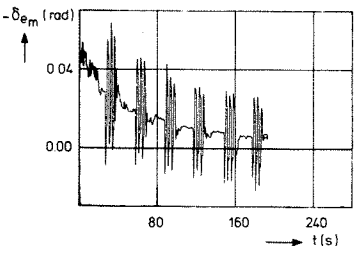

FIG. 5.1: RECORDED TIME HISTORY $\delta_{em}(t)$.

5.3 The aerodynamic model

It may be deduced from the previous sections that the flight test method centers around the specification and identification of a mathematical model of the total aerodynamic force in the plane of symmetry, the aerodynamic moment about the Y-axis and of engine thrust. The mathematical model and model parameter estimation is described in [27].

5.4 Experimental results

The techniques described in Section 3 have also been applied to the analysis of flight test data resulting from the Hawker Hunter flight test program. Presentation of the flight test results is restricted in this section to those obtained by correcting the measurements in quasi-steady, nominally horizontal accelerated flight to steady straight climbing flight - and a set of standard flight conditions. In this case the corrections required have been computed setting the Mach number M_2 equal to M_1.

Results are presented in Fig. 5.2, showing curves representing rate of climb as a function of airspeed as derived from 9 flight test maneuvers at 10.000 20.000 and 30.000 ft nominal flight altitude and corrected to a set of nominal "standard" values of aircraft weight, centre of gravity location and engine rpm.

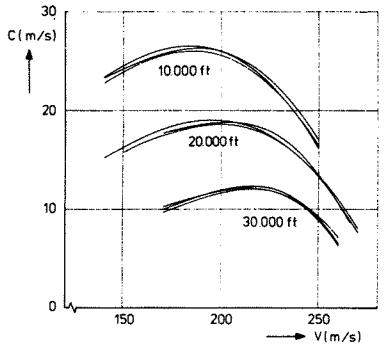

FIG 5.2. RATE OF CLIMB AS A FUNCTION OF AIRSPEED; ACTUAL FLIGHT TEST MEASUREMENTS.

As may be deduced from this figure, the scatter of the curves presented is in the order of 0.2 m/s. The repeatability of these characteristics may be concluded to be comparable to the estimated sample standard deviation of similar characteristics obtained by flight testing the De Havilland DHC-2 Beaver, see Fig. 4.4.

As already stated in the previous sections, correction of quasi-steady to steady flight conditions may yield other characteristics as well. As engine thrust could be accurately measured the polar drag curve could be derived. Correcting for Reynolds number effects and base drag variation the polar drag curves obtained showed a remarkable repeatability [27].

Section 6. Conclusions and suggestions for further research

The present paper stresses the concepts of the flight test technique discussed rather than experimental results obtained by flight testing up-to-date aircraft.

From the data shown in the previous sections it may be concluded that the estimation procedure comprising the Kalman filter- and Kalman fixed interval smoothing algorithm, can successfully be applied to flight path reconstruction from on-board measurements in nonsteady flight.
The still not commonly recognized fact, that aircraft steady state performance characteristics can be accurately derived from quasi-steady flight conditions is clearly established by the results shown.

A drastic reduction in the flight time required for performance, stability and control testing may be expected achievable when using the nonsteady flight test method discussed.

Flight path reconstruction accuracy and the repeatability of the characteristics subsequently derived are for the approximately rigi aircraft tested, shown to be limited by both steady and nonsteady atmospheric motions as well as to a certain extent by thrust modelling errors.

Further research should reveal what measurement- and data analysis techniques are required for accurate determination of performance, stability and control characteristics from nonsteady flight measurements when testing large flexible, transonic or supersonic flight vehicles.

References

1. Hussenot; "Méthodes Nouvelles d'Essais en Vol", Techniques et Science Aeronautique, Vol. 6. pp. 38-49, 1950.
2. Vleghert, J.P.K.; "Measuring climb performance of a propeller engined transport aeroplane using the acceleration technique", AGARD Report 127, 1957.
3. Gerlach, O.H.; "Analyse van een mogelijke methode voor het meten van prestaties en stabiliteits- en besturingseigenschappen van een vliegtuig in niet-stationaire, symmetrische vluchten", (in Dutch with summary in English), Delft University of Technology, Department of Aerospace Engineering, Delft, Report VTH-117, 1964.
4. Klopfenstein, H.B.; "Obtaining airplane drag data from nonsteady flight", AIAA Paper, no. 65-211, 1965.
5. Touraille, J., Langlade, R.; "Mésure des performances - méthodes d'essais en vol appliquées à Concorde", AGARD Conference Proceedings, no. 85, 1971.
6. Gerlach, O.H.; "The determination of stability derivatives and performance characteristics from dynamic maneuvers", AGARD Conference Proceedings, no. 85, 1971.
7. Gerlach, O.H.; "Determination of performance and stability parameters from nonsteady flight test maneuvers", Society of automotive engineers, Inc., National business aircraft meeting, Wichita, Kansas, SAE Paper no. 700236, 1970.
8. Hosman, R.J.A.W.; "A method to derive angle of pitch, flight-path angle and angle of attack from measurements in nonsteady flight", Delft University of Technology, Department of Aerospace Engineering, Delft, Report VTH-156, 1971.
9. Mulder, J.A.; "Aircraft performance measurements in nonsteady flights", Proceedings 3rd IFAC Symposium on "Identification and system parameter estimation", Delft-The Hague, 1973.
10. Jonkers, H.L.; "Application of the Kalman filter to flight path reconstruction from flight test data including estimation of instrumental bias error corrections", Delft University of Technology, Department of Aerospace Engineering, Delft, Report VTH-162, 1976.
11. Mulder, J.A.; "Measurement of performance, stability and control characteristics of an aircraft in nonsteady symmetric flight", Delft University of Technology, Department of Aerospace Engineering, Delft, Report VTH-157 (to be published).
12. Mulder, J.A.; "Estimation of thrust and drag in nonsteady flight", Proceedings 4th IFAC Symposium on "Identification and system parameter estimation", Tbilisi, USSR, September 1976.
13. Sage, A.P., Melsa, J.L.; "Estimation theory with applications to communications and control", McGraw-Hill, New York, 1971.
14. Mulder, J.A.; "Estimation of the aircraft state in nonsteady flight", AGARD Conference Proceedings, no. 172, 1974.
15. Etkin, B.; "Dynamics of atmospheric flight", John Wiley and Sons, Inc., New York, London, Sydney, Toronto, 1971.
16. Jazwinski, A.H.; edited by R. Bellman, "Stochastic processes and filtering theory", Academic Press, Inc., New York, London, 1970.
17. Sorenson, H.W.; "Kalman filtering techniques", edited by C.T. Leondes, "Advances in control systems, Vol. 3", Academic Press, Inc., New York, London, 1966.
18. Kwakernaak, H., Sivan, R.; "Linear optimal control systems", Wiley-Interscience, Inc., New York, London, Sydney, Toronto, 1972.
19. Fagin, S.L.; "Recursive linear regression theory optimal filter theory, and error analysis of optimal systems", IEEE International Convention Record, Part 1, Session 30, pp. 216-240, 1964.
20. Jonkers, H.L.; "A survey of five recursive minimum variance estimation procedures", Delft University of Technology. Department of Aerospace Engineering, Delft, Report M-155, 1970.
21. Smillie, K.W.; "An introduction to regression and correlation", Academic Press, Inc., New York, London, 1966.
22. Deutsch, R.; "Estimation theory", Prentice Hall, Inglewood Cliffs, New Jersey, 1965.
23. Fraser, D.C.; "A new technique for the optimal smoothing of data", Massachusetts Institute of Technology, Report T-474, 1967.
24. Kleingeld, H.W.; "Design and evaluation of a symmetric flight-test maneuver for the estimation of longitudinal performance and stability and control characteristics", AGARD Conference Proceedings, no. 172, 1974.
25. Hosman, R.J.A.W.; "Advanced flight test instrumentation: design and calibration", AGARD Conference Proceedings, no. 172, 1974.
26. Jonkers, H.L., Mulder, J.A., Van Woerkom, K.; "Measurements in nonsteady flight: Instrumentation and analysis", Proceedings of the 7th International Aerospace Instrumentation Symposium, Cranfield, 1972.
27. Mulder, J.A.; "Estimation of drag and thrust of jet-propelled aircraft by nonsteady flight test maneuvers", AGARD FMP Symposium on Flight Test Techniques, Porz-Wahn, October, 1976.